2009 American Control Conference
Hyatt Regency Riverfront, St. Louis, MO, USA
June 10-12, 2009



# Dynamics and Control of Membrane Hydration in a PEMFC*

Syed Ahmed and Donald J. Chmielewski†

## Abstract

*The subject of water management is a key issue in the design and operation of Polymer Electrolyte Membrane Fuel Cells (PEMFC). In this paper we present a dynamic model central to understanding the water management and flooding issue. First we consider membrane hydration and show how the interplay between electro-osmotic drag and back-diffusion determine ionic conductivity. The model is then used to identify appropriate manipulated variables for controlling the location and shape of the hydration profile within the membrane.*

## 1. Introduction

The overall objective of a PEMFC control system is to deliver power at levels equal to that requested by a command signal (presumably coming from the cell user or a higher level controller), which suggests that achieving a wide range of possible power conditions is of fundamental concern. In this note we illustrate how the phenomena of membrane dehydration and GDL flooding create limitations to the set of available power conditions. We also pursue the question of finding new manipulated variables capable of changing the membrane hydration profile.

As one would expect the literature on fuel cell modeling is quite large, for an overview please see the following texts: [1, 2]. Concerning membrane hydration models the work of Springer et.al [3] is fundamental. In addition to [3], the current hydration model employs techniques from [4–7]. For a variety of perspectives on the analysis and design of control systems for the PEMFC application, please see [8–14] and the references therein.

*Center for Electrochemical Science & Engineering Department of Chemical & Biological Engineering,Illinois Institute of Technology, Chicago, IL 60616

†Corresponding author:phone: 312-567-3537, fax: 312-567-8874, email: chmielewski@iit.edu

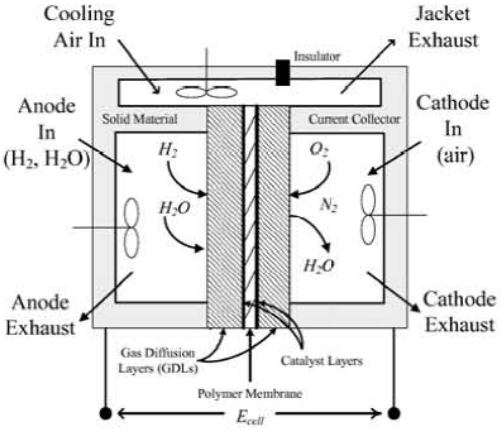


**Figure 1. Schematic of the PEMFC System.**

## 2. The Dynamic Model

The system scenario is similar to that of Lauzze and Chmielewski [9]. In contrast to [9], the new model will consider a non-pure hydrogen feed (with an exit flow) as well as hydration dynamics within the membrane.

The unit cell of the model consist of two gas chambers separated by a membrane electrode assembly (MEA), see figure 1. On the anode side, hydrogen is split into hydrogen ions and electrons. While the ions travel through the membrane, the electrons travel through the anode to the current collector and on to the load. These electrons then travel back to the cathode where they combine with the hydrogen ions and oxygen to produce water. The rate of reaction is proportional to the current density $\frac{j}{n\mathcal{F}} = -r_{H_2} = -\frac{1}{2}r_{O_2} = r_{H_2O}$ where $r_i$ represents the generation of species $i$ per unit area. While the membrane is designed to be impermeable to $H_2$ and $O_2$, it is capable of significant water uptake. As such $r_{H_2O}$ cannot be used for the gas phase material balances. Instead we define a pair of water transfer fluxes to the membrane from the anode and cathode gas chambers, $J^a_{H_2O}$ and $J^c_{H_2O}$.

## 2.1. Material and Energy Balances

In the anode chamber:

$$V_a \frac{dC^a_{H_2}}{dt} = F^a_o C^a_{H_2,o} - F^a_1 C^a_{H_2} + r_{H_2} A_m \quad (1)$$

$$V_a \frac{dC^a_{H_2O}}{dt} = F^a_o C^a_{H_2O,o} - F^a_1 C^a_{H_2O} - J^a_{H_2O} A_m \quad (2)$$

$$V_a \frac{dT^a}{dt} = F^a_o T^a_o - F^a_1 T^a + \frac{(UA)_a}{c_{ig}\tilde{C}_{p,ig}}(T^s - T^a) + (r_{H_2} T^a - J^a_{H_2O} T^a) A_m / C_{ig} \quad (3)$$

$$F^a_1 = F^a_o + (r_{H_2} - J^a_{H_2O}) A_m / C_{ig} \quad (4)$$

in the cathode chamber:

$$V_c \frac{dC^c_{O_2}}{dt} = F^c_o C^c_{O_2,o} - F^c_1 C^c_{O_2} + r_{O_2} A_m \quad (5)$$

$$V_c \frac{dC^c_{H_2O}}{dt} = F^c_o C^c_{H_2O,o} - F^c_1 C^c_{H_2O} - J^c_{H_2O} A_m \quad (6)$$

$$V_c \frac{dT^c}{dt} = F^c_o T^c_o - F^c_1 T^c + \frac{(UA)_c}{c_{ig}\tilde{C}_{p,ig}}(T^s - T^c) + (r_{O_2} T^c - J^c_{H_2O} T^s) A_m / C_{ig} \quad (7)$$

$$F^c_1 = F^c_o + (r_{O_2} - J^c_{H_2O}) A_m / C^c_{ig} \quad (8)$$

At the solid material and cooling jacket:

$$V_j \frac{dT^j}{dt} = F^j T^j_o - F^j T^j_1 + \frac{(UA)_j}{(\rho C_p)_j}(T^s - T^j) \quad (9)$$

$$(\rho\tilde{C}_p)_s V_s \frac{dT^s}{dt} = (UA)_a (T^a - T^s) + (UA)_c (T^c - T^s) + (UA)_j (T^j - T^s) + (UA)_e (T^e - T^s) - (r_{H_2} T^a + r_{O_2} T^c - J^a_{H_2O} T^a - J^c_{H_2O} T^s) A_m \tilde{C}_{p,ig} + Q_{gen} A_m \quad (10)$$

The heat generation term $Q_{gen}$ is the amount of heat produced by the electrochemical reaction, given by $Q_{gen} = (\Delta H_{f,H_2O}) r_{H_2O} - P_e$, where $P_e = jE_{cell}$.

## 2.2. Electrochemical Model

The cell voltage is the ideal losses

$$E_{cell} = E_{ner} - E_{act} - E_{ohm} - E_{mt} \quad (11)$$

$E_{ner} = E^o + (RT^{(s)}/n\mathscr{F}) ln(P_{H_2} P^{\frac{1}{2}}_{O_2} / P_{H_2O})$ is the Nernst potential. The activation loss is $E_{act} = (1/\alpha)(RT^{(s)}/n\mathscr{F}) ln(j/j_o)$, where $j_o = j^o_o (C^c_{O_2}/C^o_{O_2})^\gamma$ is the exchange current density. The ohmic loss is $E_{ohm} = jA_m \mathscr{R}$, where $\mathscr{R} = \int_0^{\delta_m} dz/\sigma(z)$, $\sigma(z) = 0.005193\lambda(z) - 0.00326 exp(1269.0(1/303 - 1/T))$, $\lambda(z) = C^m_{H_2O}(z)/N_s$ and $C^m_{H_2O}(z)$ is the membrane hydration level within the membrane (defined in the next section). $\delta_m$ is the membrane thickness ($z = 0$ is anode side and $z = \delta_m$ is the cathode side). The mass transfer loss is $E_{mt} = (1/2 + \gamma/\alpha)(RT^{(s)}/n\mathscr{F}) ln(j_L/(j_L - j))$, where $j_L = 2n\mathscr{F} k^c_{gdl} C^c_{O_2}$ is the limiting current density. The mass transfer coefficient across the GDL is $k^i_{gdl} = D^i_{gdl}/\delta^i_{gdl}$ where $\delta^i_{gdl}$ is the thickness of the GDL, $D^i_{gdl} = \varepsilon^{1.5} 0.1775 (T/273.15)^{1.823}$, $\varepsilon_i$ is the GDL void fraction and $i = c$ or $a$.

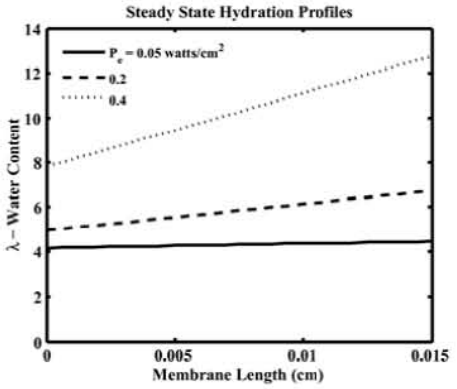


**Figure 2. Typical water content profiles.**

## 2.3. Membrane Hydration Model

A water balance within the membrane yields:

$$\frac{\partial C^m_{H_2O}}{\partial t} = -\frac{\partial J^m_{H_2O}}{\partial z} \quad (12)$$

where $C^m_{H_2O}$ is the concentration of water in the membrane and $J^m_{H_2O}$ is the flux of water through the membrane. Water transport within the membrane is due to two separate mechanisms- diffusion and electro-osmotic drag. $J^m_{H_2O} = J_{df} + J_{dg}$, where

$$J^m_{H_2O} = -D_m \frac{\partial C^m_{H_2O}}{\partial z} + \xi \frac{j}{\mathscr{F}} \quad (13)$$

If we assume the diffusion and drag coefficients ($D_m$and $\xi$)are constant, the following model will arise.

$$\frac{\partial C^m_{H_2O}}{\partial t} = D_m \frac{\partial^2 C^m_{H_2O}}{\partial z^2} \quad (14)$$

$$J^a_{H_2O} + D_m \frac{\partial C^m_{H_2O}}{\partial z} - \frac{j\xi}{\mathscr{F}} = 0 \text{ at } z = 0 \quad (15)$$

$$-D_m \frac{\partial C^m_{H_2O}}{\partial z} + \frac{j\xi}{\mathscr{F}} + J^c_{H_2O} + r_{H_2O} = 0 \text{ at } z = \delta_m \quad (16)$$

The flux of water entering the membrane from the gas chambers is

$$J^a_{H_2O} = k^a_{gdl}\left[C^a_{H_2O} - \hat{C}^a\right] \quad (17)$$

$$J^c_{H_2O} = k^c_{gdl}\left[C^c_{H_2O} - \hat{C}^c\right] \quad (18)$$

where $\hat{C}^i = a^i_w [(P_{vap}(T^s)/RT^s)]$ and $a^i_w$ satisfies the gas / membrane equilibrium relation at the chamber interfaces, determined by

$$N_s\left(0.043 + 17.81a^a_w + 39.85(a^a_w)^2 + 36.0(a^a_w)^3\right) = C^m_{H_2O}\Big|_{z=0} \quad (19)$$

$$N_s\left(0.043 + 17.81a^c_w + 39.85(a^c_w)^2 + 36.0(a^c_w)^3\right) = C^m_{H_2O}\Big|_{z=\delta_m} \quad (20)$$

Figure 2 illustrates typical water content profiles, all at steady state and a solid temperature of 80°C. At the low power condition, we see that diffusion dominates (indicated by the nearly horizontal profile). However, at the higher power condition we see the combined effect of water generation on the cathode side along with electro-osmotic drag, also toward the cathode side.

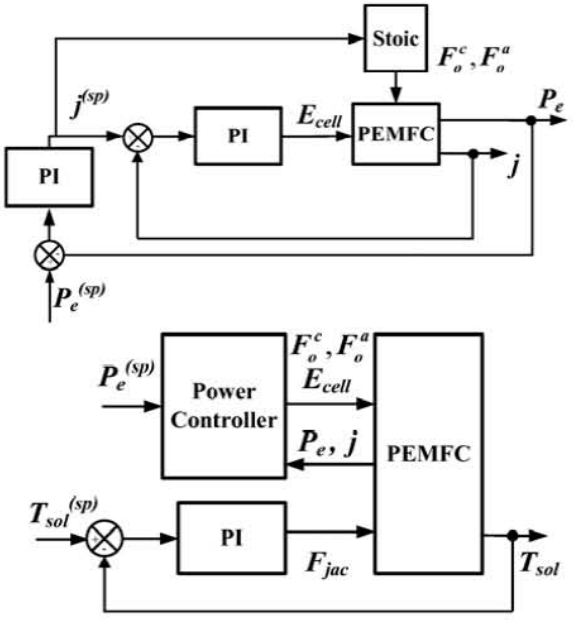


**Figure 3. Power / Temperature Control Loops**

In the event of flooding ( $a_w^c \geq 1$) , the mass transfer coefficient at the cathode, $k_{gdl}^c$, is modified to

$$k_{gdl}^c = (D_{gdl}^c/\delta_{gdl}^c)[1 - F_o exp(((N_{gdl}^{H_2O}/N_{gdl}^{max}) - 1)/\psi)]$$

where $F_o$, and $\psi$ are porosity and antiflooding coefficients, $N_{gdl}^{H2O}$ is amount of water present in the GDL and $N_{gdl}^{max}$ is the maximum the GDL can hold. The amount of water in the GDL is given by:

$$\frac{1}{A_m}\frac{dN_{gdl}^{H2O}}{dt} = J_{fl} - A_{gdl}k_{gdl}^c * (\tilde{C}^c - C_{H2O}^c) \quad (21)$$

where $A_{gdl} = \phi N_{H2O}^{gdl}$is the surface area available for water evaporation from the GDL. The flux of liquid water being ejected from the membrane is given by $J_{fl} = K_{fl} * \max[0, (C_{H_2O}^m/N_s - 14)]$. To complete the flooding model we need only subtract $J_{fl}$ from the left side of (16). $F_o$,$\psi$,$\phi$,$K_{fl}$ and $N_{gdl}^{max}$ are parameters of the GDL to be determined empirically.

## 3. Temperature Control

Using the feedback structure of figure 3, we simulate the fuel cell responses to increasing and decreasing step changes in the power set-point. Consider the 10 - 200 second interval of figure 4. The increase in power causes the solid temperature to increase, which causes the controller to increase jacket flow, and thus bring the temperature back to set-point.

This return to the set-point causes the water removal driving forces to remain about constant, which results in a net increase in water content within the membrane, due to increased generation and electro-osmotic drag. In the second two intervals (200 - 450 and 450-600 seconds), similar responses are observed, with the exception of the flooding event at about 600 seconds, which results in the unstable behavior observed.

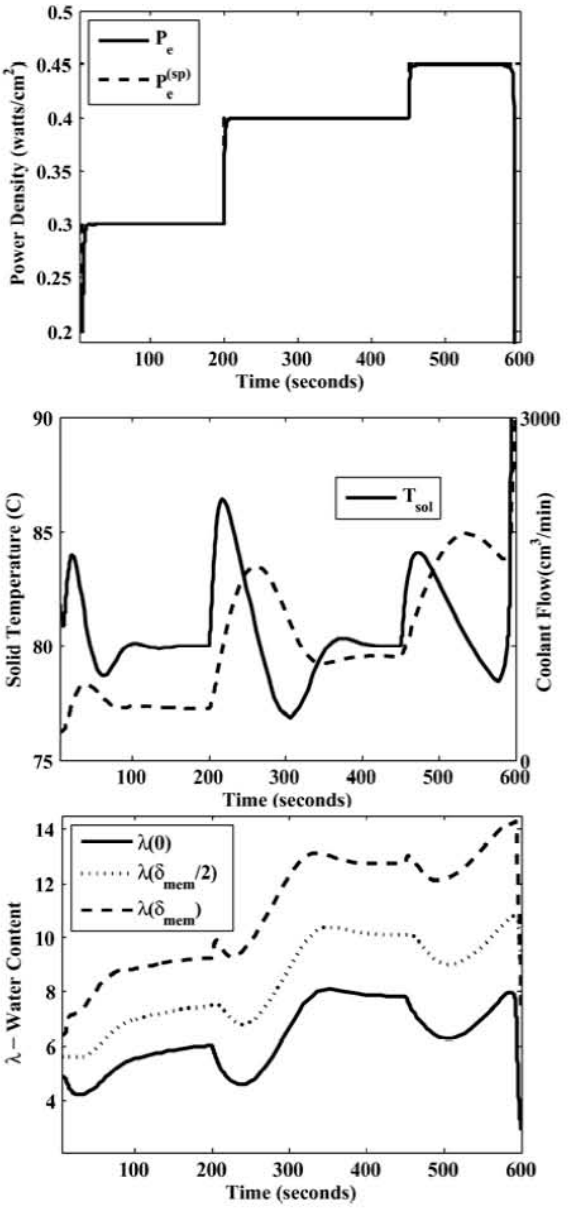


**Figure 4. Response to Power Increases**

In figure 5, the opposite responses occur. Although the cell is not expected to fail, the fairly low hydration level within the membrane (and thus low ionic conductivity) suggests fairly inefficient operation. It is also noted that the closed-loop settling time with respect to temperature is around 50 seconds, and the open-loop

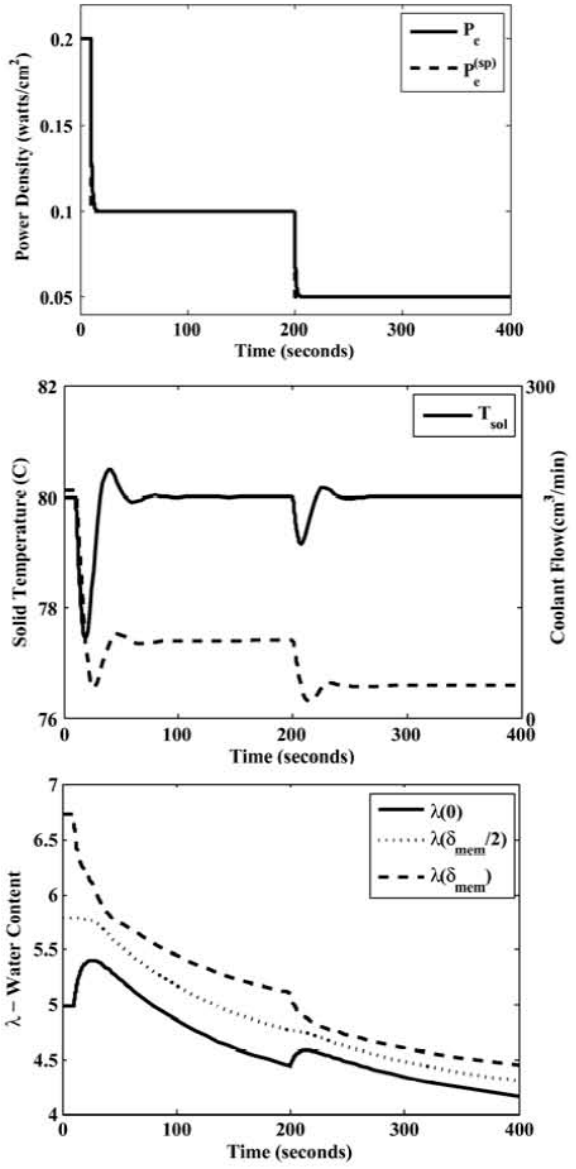


**Figure 5. Response to Power Decreases**

settling time for membrane hydration is around 200 seconds.

## 4. Manipulation of the Hydration Profile

As indicated in the previous section, changes in power output will dramatically influence the water content profile within the membrane. The first concern is average water content. At high power, the average increases, while at low it decreases. Both of these conditions have detrimental results, flooding in the first case and dehydration in the second. The second concern is profile shape. Consider the high power case of figure

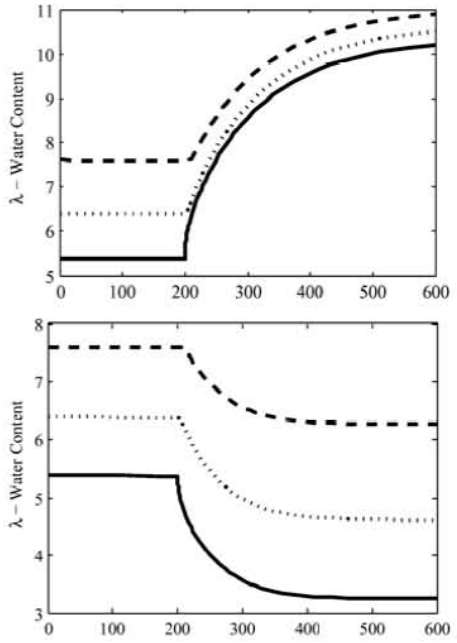


**Figure 6. Step responses due to anode bubbler temperature (upper plot, 86$^o$C to 90$^o$C, lower plot, 86$^o$C to 82$^o$C )**

4. In addition to an increase in average water content, we see an increase in the slope. From an ohmic loss/efficiency perspective, the ideal profile has zero slope and is just below the flooding condition $\lambda$=14. This brings us to a fundamental question: Does there exist a set of manipulated variables that can influence the position and slope of the hydration profile?

To address this question we identified a number potential manipulations. These include: anode bubbler temperature, cathode bubbler temperature, and the solid setpoint temperature. In the step tests to follow we impose a constant current condition ($j$=0.2 A/cm$^2$) so as to decouple the reaction rate and ionic conductivity relationship.

In figure 6, an increase in anode bubbler temperature (from 86$^o$C to 90$^o$C) not only increases the average water content, it also reduces the slope. Since it is assumed that gas leaving the bubbler is saturated, an increase in bubbler temperature has the effect of increasing gas water content at the anode inlet. This causes an increase in the flux of water from the anode gas to anode side of the membrane. The net effect is a lifting of the anode side water content which also serves to increase the average. It should be noted that an increase in bubbler temperature will increase the inlet and thus anode gas temperature, which will decrease the water flux driving force. Based on the simulation results, this

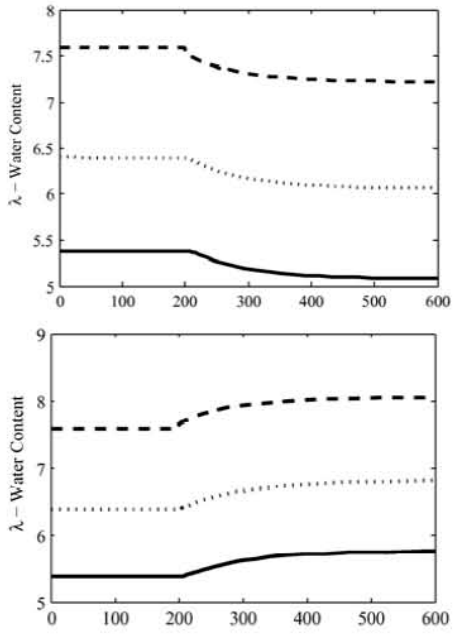


**Figure 7. Step responses due to cathode bubbler temperature (upper plot, 40$^o$C to 50$^o$C, lower plot, 40$^o$C to 30$^o$C)**

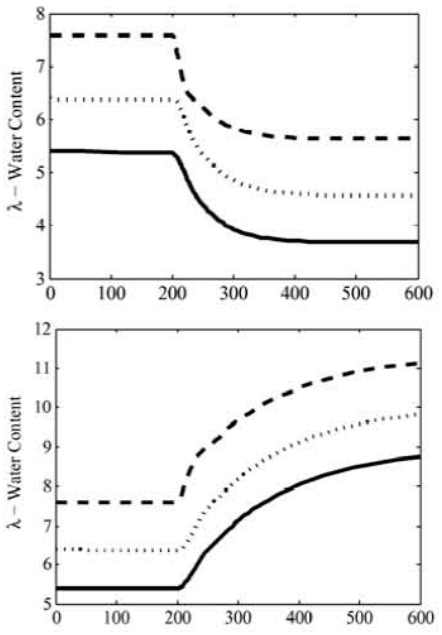


**Figure 8. Step responses due to set-point temperature (upper plot, 80$^o$C to 70$^o$C, lower plot, 80$^o$C to 90$^o$C)**

change has a much smaller impact compared to the water content of the gas.

Concerning the cathode bubbler (figure 7), the impact is much less dramatic and the gain is of opposite sign. We attribute this to the larger impact of changing inlet gas temperature verses that of water content. In essence the two competing effects of bubbler temperature almost cancel each other at the cathode. This stronger impact of inlet gas temperature at the cathode is due to the larger cathode gas flow which results in more influence on gas temperature within the chamber.

Changes to the solid temperature set-point will impact the average membrane water content, but will leave the slope essentially unchanged (see figure 8). This stems from the fact that the gas temperature in both chambers will be influenced equally. Thus, the water flux driving force will be impacted equally on both sides of the membrane.

Summarizing the step responses, we find that the anode bubbler temperature can decrease slope, but will also increase average membrane water content. The cathode bubbler temperature can also change average water content, but does so at a much smaller gain and has little impact on slope. Finally, solid temperature has a strong influence on average water content with almost no change to the slope. This suggests the following open-loop control scheme; simultaneously increase

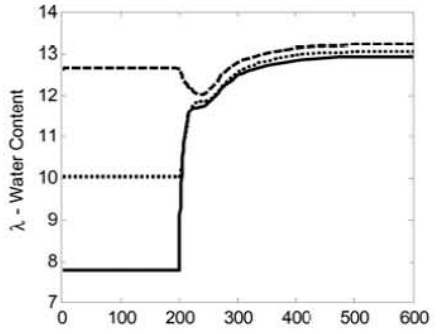


**Figure 9. Combined anode bubbler and set-point temperature increase**

anode bubbler temperature (to flatten slope), while decreasing solid temperature (to stay out of the flooding regime). Figure 9 shows such simulation.

## 5. Conclusions

Clearly this is only a portion of the puzzle. Before one can close the loop, a suitable set of measurements (capable of inferring the hydration profile) would need to be identified. Such a measurement scheme will likely include a combination of online impedance spectroscopy (to measure ionic resistance and infer average water in the membrane) along with a model based state

estimator, driven by more traditional measurements of temperature, relative humidity and gas flow rates. An additional complication is the along the channel component of the fuel cell. Clearly, the conclusions of this CSTR based study would need to be revalidated within such a configuration.

## 6. Acknowledgements

This work was supported by the Department of Chemical and Biological Engineering and the Graduate College at the Illinois Institute of Technology.

## 7. Notation

| | |
|---|---|
| super- | and sub-scripts |
| $a, c, j, e$ | anode, cathode, jacket, ambient gas |
| $s, m$ | solids, membrane |
| $C$ | Concentrations(mol/cm$^3$) |
| $T$ | Temperature(K) |
| $F_0, F_1$ | Inlet and Outlet Flows(cm$^3$/s) |
| $r_{H_2}, r_{O_2}$ | Reaction rate of Hydrogen, Oxygen |
| $A$ | Area(cm$^2$) |
| $V$ | Volume(cm$^3$) |
| $\lambda$ | Water Profile in Membrane |
| $U$ | Heat Exchanger Coef.(J/s-cm$^2$-K) |
| $C_{ig}$ | Ideal Gas Concentration(mol/cm$^3$) |
| $\tilde{C}_{p,ig}$ | Ideal Gas Heat Capacity(J/mol-K) |
| $N_s$ | Number of Sulfonic Sites(mol/cm$^3$) |
| $Q_{gen}$ | Heat Generation |
| $j$ | Current Density(A/cm$^2$) |
| $E_{cell}$ | Voltage of Fuel Cell(V) |
| $\Delta H_{f,H_2O}$ | Heat of Formation of Water(J/mol) |
| $n$ | No. of electrons transferred in reaction |
| $\alpha$ | Charge transfer coefficient |
| $j_o$ | Exchange current density |
| $j_o^o$ | Exchange current density at reference concentration |
| $C_{O_2}^o$ | Reference Concentration |
| $\gamma$ | Activity coefficient |
| $\mathscr{R}$ | Resistance of Membrane |
| $\sigma$ | Conductivity in Membrane |
| $D_m$ | Membrane diffusion Coefficient |
| $D_{gdl}^c$ | Diffusion constant across GDL |
| $F_o$ | Empirical Parameter for GDL |
| $\psi$ | Empirical Parameter for GDL |
| $J_{fl}$ | Flux of liquid ejected from Membrane |
| $K_{fl}$ | Empirical Parameter for GDL |
| $N_{gdl}^{H_2O}$ | Moles of Water in GDL |
| $N_{gdl}^{H_2O,max}$ | Maximum Moles of Water in GDL |

## References

[1] Larminie, J., and A. Dicks. *Fuel Cell Systems Explained*. 2nd ed. West Sussex: John Wiley & Sons, 2003.

[2] O'Hayre, R., S-W. Cha, W. Colella, and F. Prinz. *Fuel Cell Fundamentals*. New York: John Wiley & Sons, 2006.

[3] Springer, T.E., T.A. Zawodzinski, and S. Gottesfeld. "Polymer Electrolyte Fuel Cell Model." *Journal of Electrochemical Society* 138 (1991):2334-2342.

[4] Zawodzinksi, T.A., J. Davey, J. Valerio, and S. Gottesfeld. "The Water Content Dependence of Electro-osmotic Drag in Proton-Conducting Polymer Electrolytes." *Electrochimica Acta* 40 (1995):297-302.

[5] Weber, A.Z., and J. Newman. "Transport in Polymer-Electrolyte Membranes." *Journal of The Electrochemical Society* 151 (2004):A311-A325.

[6] Weber, A.Z., and J. Newman. "Modeling Transport in Polymer-Electrolyte Fuel Cells." *American Chemical Society* 104 (2004):4679-4726.

[7] Chen, F.,H.S. Chu, C.Y. Soong, and W.M. Yan. "Effective Schemes to Control the Dynamic Behavior of the Water Transport in the Membrane of PEM Fuel Cell." *Journal of Power Sources* 140 (2005):243- 249.

[8] Pukrushpan, J.T., A.G Stefanopoulou, and H. Peng. *Control of Fuel Cell Power Systems: Principles, Modeling, Analysis and Feedback Design*. London: Springer-Verlag, 2004.

[9] Lauzze, K.C., D.J. Chmielewski. "Power Control of a Polymer Electrolyte Membrane Fuel Cell." *Industrial & Engineering Chemistry Research* 45 (2006):4661-4670.

[10] Golbert, J., D.R. Lewin. "Model-Based Control of Fuel Cells (2): Optimal Efficiency." *Journal of Power Sources* 173 (2007):298-309.

[11] Methekar, R.N., V. Prasad, and R.D. Gudi. "Dynamic Analysis and Linear Control Strategies for Proton Exchange Membrane Fuel Cell using a Distributed Parameter Model." *Journal of Power Sources* 165 (2007):152-170.

[12] Yang, Y., F.C. Wang, H.P. Chang, Y.W. Ma, and B.J. Weng. "Low Power Proton Exchange Membrane Fuel Cell System Identification and Adaptive Control." *Journal of Power Sources* 164 (2007):761-771.

[13] Zenith, F. *Control of Fuel Cells*. Diss. Norwegian Univ. of Science and Technology, 2007. Trondheim: NTNU-Trykk, 2007.

[14] Zhang, L., M. Pan, and S. Quan. "Model predictive control of water management in PEMFC." *Journal of Power Sources* 180 (2008):322-329.